Performance evaluations and applications of a δ^{13}C-DIC analyzer in seawater and estuarine waters

Xue Deng [a,b,c], Qian Li [a], Jianzhong Su [a,d], Chun-Ying Liu [b], Eliot Atekwana [e], Wei-Jun Cai [a,*]

[a] School of Marine Science and Policy, University of Delaware, Newark, DE 19716, USA
[b] Frontiers Science Center for Deep Ocean Multispheres and Earth System, Key Laboratory of Marine Chemistry Theory and Technology, Ministry of Education, College of Chemistry and Chemical Engineering, Ocean University of China, Qingdao 266100, PR China
[c] Key Laboratory for Ecological Environment in Coastal Areas (State Oceanic Administration), National Marine Environmental Monitoring Center, Dalian 116023, China
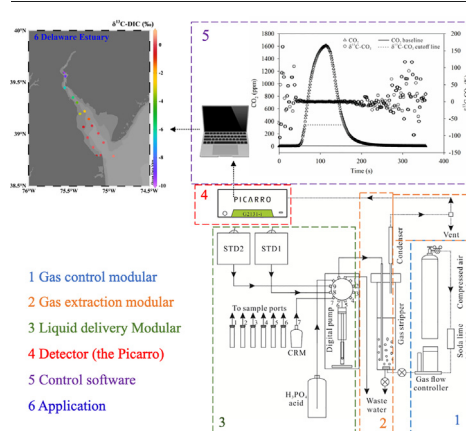[d] State Key Laboratory of Marine Resources Utilization in South China Sea, Hainan University, Haikou 570228, China
[e] Earth and Planetary Sciences Department, University of California Davis, Davis, CA 95616, USA

HIGHLIGHTS

- Instrument and technique to simultaneously and precisely measure DIC and δ^{13}C-DIC.
- Instrument is portable and can be deployed at field sites and onboard ships.
- Suggestions on how to precisely analyze δ^{13}C-DIC sample with different DIC contents.
- The system will enhance spatiotemporal near real-time analysis of DIC and δ^{13}C-DIC.

GRAPHICAL ABSTRACT

1 Gas control modular
2 Gas extraction modular
3 Liquid delivery Modular
4 Detector (the Picarro)
5 Control software
6 Application

ARTICLE INFO

ABSTRACT

Dissolved inorganic carbon (DIC) and its stable isotope (δ^{13}C-DIC) are important parameters for studying carbon cycling in aquatic environments. Traditional methods based on isotope-ratio mass spectrometers are labor-intensive and not easily deployable at field sites. Here we report the performance of a method that simultaneously measures DIC concentration and its stable isotope by using a CO_2 extraction device and a Cavity Ring-Down Spectroscopy (CRDS) detector. A multi-port valve is used to increase sample throughput and improve precision. The instrument achieves average precisions of better than $\pm 1.95\ \mu mol\ kg^{-1}$ and $\pm 0.06‰$, respectively, for DIC and δ^{13}C-DIC in seawater based on three injections for each sample. We also provide recommendations on how to precisely determine δ^{13}C-DIC samples with a wide range of DIC content in different types of waters by examining injection volume and concentration effects. This technique was applied to study carbon cycling in the Delaware Estuary. It demonstrates that a simultaneous and precise determination of both DIC and δ^{13}C-DIC is a powerful and effective approach for constraining the processes controlling aquatic carbon cycling and CO_2 fluxes. Both laboratory tests and field applications confirmed that this system can be used with high precision to study carbon cycling in various aquatic environments.

* Corresponding author.
E-mail address: wcai@udel.edu (W.-J. Cai).

1. Introduction

Dissolved inorganic carbon (DIC) is the primary carbon pool in natural waters and its quantification is essential for studying the global carbon cycle. The stable isotope of DIC (δ^{13}C-DIC) is a powerful tool for determining the sources and sinks of DIC and in understanding carbon cycling and the associated biogeochemical processes in aquatic ecosystems (Alling et al., 2012; Hellings et al., 1999; Samanta et al., 2015; Schulte et al., 2011; Su et al., 2017, 2019; Wang et al., 2016; Xuan et al., 2020). In particular, the δ^{13}C-DIC can be used to elucidate whether the source of DIC is allochthonous or autochthonous and can be used to separate the relative contributions among different pools of organic matter degradation, biological production, and physical processes that control DIC dynamics in the ocean and coastal waters (Alling et al., 2012; Bhavya et al., 2018; Gruber et al., 1998; Quay et al., 2009; Samanta et al., 2015). In addition, the δ^{13}C-DIC is a useful tracer in determining anthropogenic CO_2 uptake rate by the ocean and can be used to identify whether an ocean region is a sink for anthropogenic CO_2 (Quay et al., 2003, 2017).

In most oceanographic and hydrogeological studies, the δ^{13}C-DIC is measured by gas source isotope-ratio mass spectrometry (IRMS). The high precision and accuracy have made IRMS the preferred conventional technique for determining δ^{13}C-DIC over the last several decades (Atekwana and Krishnamurthy, 2004; Humphreys et al., 2015; Salata et al., 2000; Torres et al., 2005; Waldron et al., 2014). However, the disadvantages of the IRMS-based conventional technique (e.g., the high level of required expertise for sample pretreatment and analysis, the complexity of equipment set-up, the expensive instrument maintenance, the inability to deploy in the field) limit the ability to conduct δ^{13}C-DIC studies with high temporal and spatial resolutions (Becker et al., 2012; Friedrichs et al., 2010). In open ocean transect cruises, water samples were collected, preserved and transported back to land-based laboratories for δ^{13}C-DIC analysis by the IRMS technique. Thus, compared to the direct DIC concentration analysis onboard for every sampling station and depth, only <15% of samples have corresponding δ^{13}C-DIC analysis (Becker et al., 2016). Therefore, lower spatial and temporal δ^{13}C-DIC coverages limit the full benefits of the δ^{13}C-DIC as a more sensitive tracer than DIC for the study of anthropogenic CO_2 uptake and biogeochemical processes (Quay et al., 2003, 2017). Finally, a lack of the flexibility of making immediate decisions on issues such as adding additional sampling stations and times based on feedbacks from onsite analysis is another obvious disadvantage of the use of the traditional IRMS method.

In recent years, extensive efforts have been made to overcome the limitations of the IRMS-based conventional technique, especially automation of sample preparation and deployability to conduct near-real-time δ^{13}C-DIC analysis. Among these, the laser-based optical spectroscopy has gained increasing recognition and is a suitable alternative approach to simultaneously measure DIC concentrations and δ^{13}C-DIC values because of its high detection sensitivity, relatively straightforward experimental set-up, and field-portability (Bass et al., 2012; Call et al., 2017; Dickinson et al., 2017a, 2017b; Liu et al., 2021; López-Sandoval et al., 2019; Su et al., 2019). For example, Bass et al. (2012) utilized a continuous, automated DIC analyzer to monitor DIC concentrations and its δ^{13}C-DIC signals in water samples. However, their method required large sample volumes (350 mL) and the precisions of ± 10 μmol kg^{-1} for DIC and ± 0.2‰ for δ^{13}C-DIC are inadequate for studying DIC processes with small variations or slow rates. Call et al. (2017) coupled a commercially available non-dispersive infrared (NDIR) CO_2 detector based DIC analyzer to a Cavity Ring-Down Spectroscopy (CRDS) isotope analyzer to determine DIC concentrations and δ^{13}C-DIC values, respectively, with high precisions of ± 1.5–2.0 μmol kg^{-1} for DIC and ± 0.14‰ for the δ^{13}C-DIC, when DIC concentrations ranged from 1000 to 3600 μmol kg^{-1}. In the approach, the NDIR detector was used to measure DIC with one injection of the sample while the CRDS detector was used to measure δ^{13}C-DIC with another injection, and the two injections had different analytical conditions (i.e., the gas flow rate was 300 mL min^{-1} in the former and 70 mL min^{-1} in the latter). The fact that this approach requires two detectors and two

different analytical procedures for DIC and δ^{13}C-DIC probably has limited its application.

As an improvement, Su et al. (2019) used one CRDS detector and a single procedure to simultaneously quantify both DIC and δ^{13}C-DIC. In this approach, 3–4 mL samples were acidified to convert DIC to CO_2 and then both DIC concentration and its carbon isotope ratio were determined by the Picarro G2131-i CRDS analyzer to achieve precisions of ± 1.5 μmol kg^{-1} for DIC and ± 0.09‰ for δ^{13}C-DIC. However, in both Call et al. (2017) and Su et al. (2019) methods, once a sample analysis is completed, an operator needs to manually load another sample, which is still labor-intensive and limits the sample throughput rate. The approaches may also limit the analytical precision due to less consistency between analyses (e.g., time interval between samples varies). Therefore, though initial results were published in Su et al. (2019), further automation, improvements, and extensive evaluations of the performance of the analytical techniques and system are needed.

In the present study, we improved the instrument's sampling procedure from a single sample valve to a multi-port valve to achieve automated multi-sample analysis with less labor-intensive monitoring and operation. The use of the multi-port valve is also expected to provide a better consistency among different samples and thus to improve the overall analytical precision. We have carried out both extensive laboratory tests and field sample analysis to evaluate the performance of the upgraded method and system. First, we examined the repeatability of the multi-port valve to ensure that all sample channels are identical in sample delivery and work consistently. Because we drew samples from the same stock of seawater, this experiment also provided a rigorous evaluation of the analytical precision and the analytical system stability. Furthermore, the sample injection volume and DIC concentration experiments were conducted to determine the injection volume range for δ^{13}C-DIC samples with different DIC concentrations in different types of aquatic environments. Finally, we demonstrated the applicability and advantages of this new CRDS-based method via a comprehensive field study of the carbonate system in the Delaware Estuary.

2. Materials and methods

2.1. Instrument structure and analytical principle

A whole-water CO_2 extraction device with a 12-port sample valve (AS-D1, Apollo Scitech, Newark, DE, USA; www.apolloscitech.com) and a CRDS isotopic detector (G2131-i, Picarro, Santa Clara, CA, USA www.picarro.com), were coupled and automated with a single software to simultaneously measure DIC concentrations and δ^{13}C-DIC signals via quantifying the CO_2 extracted from acidified samples (Fig. 1). The principle of a previous version of this system was described in Su et al. (2019). Briefly, an aliquot of sample is acidified with 5% H_3PO_4 in the gas stripping reactor and the liberated CO_2 is brought by the carrier gas (CO_2-free compressed air) to the CRDS analyzer, where DIC concentration and δ^{13}C-DIC signal are determined simultaneously. We improved the Su et al. (2019) method by including a 12-port valve (Fig. 1). One of the sample ports is designated for the DIC standard, such as using a Certified Reference Material (CRM) or a secondary house standard to create a working standard curve for DIC calibration. Two home-made isotope standards, STD1 (-2.70‰) and STD2 (-19.57‰) were made by dissolving NaHCO$_3$ solids in deionized water, and along with CRM were used to calibrate the δ^{13}C-DIC data. The δ^{13}C-DIC values of the home-made isotope standards and CRM solution were verified by the IRMS technique in the stable isotope facility at the University of California, Davis. In an environment with narrow ranges of DIC concentration and δ^{13}C-DIC such as that in seawater (1800—2300 μmol kg^{-1} in DIC and -3 to 2‰ in δ^{13}C-DIC), a single pre-calibrated standard may be enough to serve as both concentration and isotope standard. However, in other environments such as in an estuary, two or even three standards for δ^{13}C-DIC may be desirable.

As described in Su et al. (2019), the area under the curve of the mole fraction CO_2 gas is integrated over time to derive a net area for quantifying DIC concentrations (also included in the upper right corner in the graphical
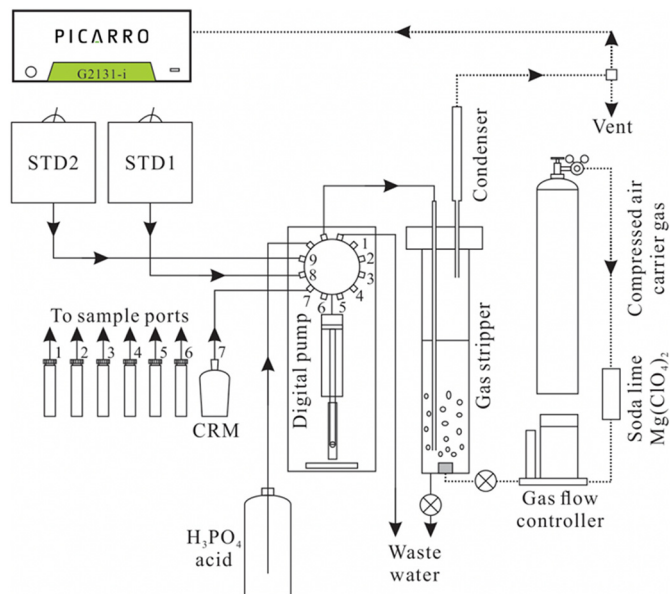
Fig. 1. A schematic layout of the CO_2 extraction device (AS-D1) and CRDS isotope detector (G2131-i) to measure DIC concentrations and $\delta^{13}C$-DIC signals autonomously and simultaneously. A 5-mL syringe is used in this work (note that the syringe volume can be changed to 10 mL). For the 12 ports valve, one port connects to the acid, one delivers the syringe's liquid to the gas stripper, one discharges to waste, ports #1 to #6 are connected to the sample lines and the rest of three ports (#7, #8 and #9) are connected to three standards (CRM, STD1 and STD2), respectively. Port #7 can be run -with a single volume or three different volumes of CRM standard for creating a DIC calibration line.

abstract). In this work, three volumes of a CRM or a home-made standard, e.g., 3.0, 3.5 and 4.0 mL, are used to create a working standard curve between the net area and DIC mole amounts. The latter is calculated as the product of the CRM or home-made standard's volume and known concentration. The DIC concentration of a sample is then derived from the working standard curve and the known injection sample volume.

The $\delta^{13}C$-DIC is derived as the CO_2 weighted mean of $\delta^{13}C$-CO_2 data. Similar to the practices in Su et al. (2019) and Call et al. (2017), we set a cutoff value to exclude $\delta^{13}C$-CO_2 at low CO_2 concentrations. This is because the Picarro instrument internally determines $\delta^{13}C$-CO_2 by referencing the ^{13}C signal to ^{12}C signal, and thus, at a very low ^{12}C signal, the $\delta^{13}C$-CO_2 signal has high noise and should not be used. A CO_2 range of 380–2000 ppm (or 1000–2000 ppm) is recommended by the manufacturer for a guaranteed isotope analysis precision of 0.1‰ (or 0.05‰) for the Picarro G2131-i. Noted that the cutoff value can be defined by users, for example, 350 ppm was set as the cutoff value in this study. As we adopted a weighted-mean method in our study, the final $\delta^{13}C$-DIC value is not particularly sensitive to the chosen cutoff value, because the noisy $\delta^{13}C$-CO_2 data at low CO_2 only accounts for a small fraction of the entire dataset.

2.2. Preparation of the stock seawater and home-made standards

The stock seawater used in all laboratory experiments was collected from the Gulf of Mexico (GoM) and had been stored in a large tank designed for research supply in the Louisiana Universities Marine Consortium (LUMCON). The seawater was filtered through 0.45 μm cartridge filter and then transferred into a 4 L gastight bag (Cali-5-Bond, Calibrated Instruments Inc.) and doped with 1 mL HgCl₂ to inhibit further biological activities, which is a standard operation protocol for preserving DIC samples (Dickson et al., 2007). Before preservation, biological respiration likely had increased DIC and decreased $\delta^{13}C$-DIC of this stock water compared

to initial values from the GoM surface waters (0.5–1.0‰; Cai laboratory unpublished data).

The home-made NaHCO₃ solution standards were similarly prepared. A certain weight of NaHCO₃ powder was dissolved in deionized water (DIC concentration about 2000 μmol L⁻¹), and then, the solution was sealed in an Al-coated gas-tight bag and was preserved with HgCl₂. Each bag was sub-sampled several times into 12-ml glass vials over the analytical period and its $\delta^{13}C$ value was late analyzed by the IRMS method at the U.C. Davis laboratory. The $\delta^{13}C$ value in such a bag does not change over at least 4 months if the solution inside the bag is more than 1/4 of the bag size (4 L). Per our method and the U.C. Davis IRMS method, as all HCO_3^- and CO_3^{2-} are acidified and converted into CO_2, the purity of the NaHCO₃ solid is not an issue of concern.

2.3. Multi-port valve test, injection volume effect and concentration effect experiments

There is the possibility for cross-contamination caused by sample carryover between subsequent ports when using a multi-port valve. Therefore, we assessed if the new multi-port system delivers identical DIC concentrations and $\delta^{13}C$-DIC values between ports. All sample and standard ports in the injection volume of 3.5 mL were connected to the same batch of stock seawater (preparation details in Section 2.2) with three consecutive injections per port to assess the multi-port valve injection consistency.

Different aquatic samples from seawater to estuarine, river and lake waters may post different challenges in sample volumes and concentration ranges. To determine if different injection volumes with the same DIC concentration or different DIC concentrations with the same injection volume could affect the measurements of DIC concentrations and $\delta^{13}C$-DIC signals using the CRDS system, we conducted the following experiments. For the injection volume effect experiment, the stock seawater in the same bag was measured in different injection volumes in a sequence from 1.2–5.8 mL at 0.2 mL increment. For the concentration effect experiment, stock seawater was diluted with CO_2-free deionized water to make a series of solutions with 7 different DIC nominal concentrations, ranging from 250 to 2300 μmol kg⁻¹, then samples were run in the same injection volume (3.5 mL), simulating waters with a wide range of DIC concentration from natural environments.

2.4. Field work in the Delaware Estuary

We evaluated the analytical method and demonstrated its applicability in the Delaware Estuary, which is composed of 100 km long tidal Delaware River and Delaware Bay (Sharp, 2010) and has a DIC range of ~1000 μmol kg⁻¹ at the river end and ~2000 μmol kg⁻¹ at the ocean end. A one-day cruise in the Delaware Estuary was conducted on April 3, 2019 (Fig. 2). The $\delta^{13}C$-DIC and ancillary parameters of surface water were collected along the longitudinal axis in the main channel and the western shoal of the Delaware Estuary to demonstrate the applicability of our DIC and $\delta^{13}C$-DIC analysis method.

The DIC and $\delta^{13}C$-DIC samples were determined by the AS-D1 $\delta^{13}C$-DIC analyzer as described above. Total alkalinity (TA) samples were measured by Gran titration with AS-ALK2 (Apollo Scitech) with a precision of ± 0.1% (Huang et al., 2012), and pH with a Ross combination electrode calibrated against three NBS buffers at 25 ± 0.1 °C with a precision of ± 0.005 pH. The DIC and TA values are reported here by referencing to the Certified Reference Material (CRM, batch 179) provided by Dr. Andrew Dickson of Scripps, U.C. San Diego. The partial pressure of CO_2 (pCO_2) was monitored by an underway pCO_2 analyzer (AS-P2, Apollo Scitech) installed in the shipboard laboratory and calibrated against three standard gases (Chen et al., 2020). Ca^{2+} samples were measured using a modified technique of Kanamori and Ikegami (1980) with a precision <0.1%. Aragonite saturation state (Ω_{Ar}) was derived by using the measured Ca^{2+}, calculated CO_3^{2-} and aragonite solubility, according to Mucci (1983).
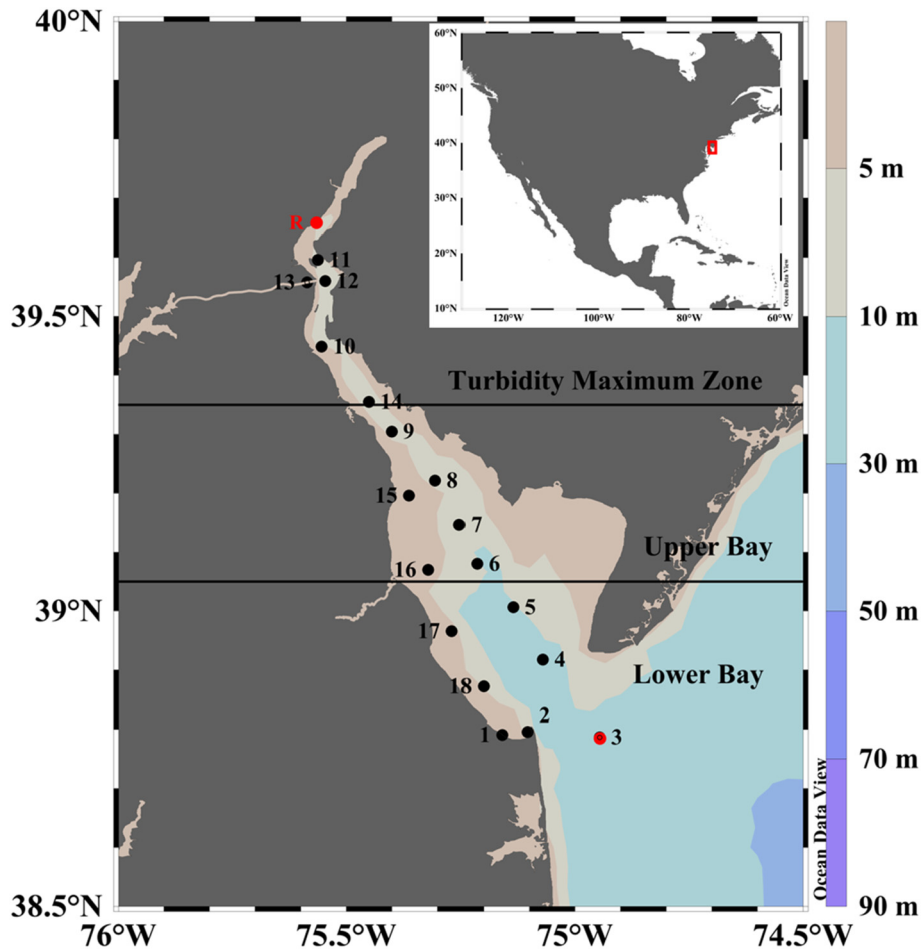
Fig. 2. Sampling stations in the Delaware Estuary. The red filled dots represent the river endmember (station R) and ocean endmember (station 3). Delaware Estuary is divided into 3 sections (turbidity maximum zone, upper bay and lower bay) by the solid horizontal lines according to Sharp et al. (2009). The inserted regional map indicates the location of the Delaware Bay on the US east coast.

2.5. Two endmember mixing calculation

The DIC concentrations and δ^{13}C-DIC values in the Delaware Estuary vary due to several processes including physical mixing, gas exchange, carbonate precipitation/dissolution and biological processes. Thus, a two-endmember mixing model is used to separate physical mixing effect from other processes. The mixing fractions between two endmembers, river water and seawater, for each sample can be quantified using salinity as a conservative tracer (Fry, 2002; Su et al., 2020):

$$f_r + f_{sw} = 1 \tag{1}$$

$$S_r \times f_r + S_{sw} \times f_{sw} = S_{meas} \tag{2}$$

$$TA_{mix} = TA_r \times f_r + TA_{sw} \times f_{sw} \tag{3}$$

$$DIC_{mix} = DIC_r \times f_r + DIC_{sw} \times f_{sw} \tag{4}$$

$$DIC_{mix} \times \delta^{13}C\text{--}DIC_{mix} = \delta^{13}C\text{--}DIC_r \times DIC_r \times f_r + \delta^{13}C\text{--}DIC_{sw} \times DIC_{sw} \times f_{sw} \tag{5}$$

where f is mixing fraction, S is the abbreviation of salinity; the subscripts r, sw, mix and $meas$ represent the river end-member, seawater end-member, conservative mixing value and the measured value of sample. Eqs. (3)–(5) are used to calculate the conservative TA, DIC and δ^{13}C-DIC mixing lines in the two-endmember mixing model. The conservative pH mixing line (at 25 °C) is calculated from the conservative DIC and TA with the CO2SYS program (Pierrot et al., 2006). The station R (Fig. 2) in the Delaware River was chosen as the river endmember, since it has near-zero salinity, is minimally affected by tidal movement in spring, and is easily accessible from a pier; Station 3 is located outside the bay mouth

Table 1
Summary information of the end-member stations in the two end-member model.

Endmembers	Latitude	Longitude	Salinity	DIC (μmol kg^{-1})	TA (μmol kg^{-1})	δ^{13}C-DIC (‰)
Riverine	39.5800°N	75.5869°W	0.16	970.6 ± 0.6	944.6 ± 0.0	−9.06 ± 0.07
Oceanic	38.7868°N	74.9459°W	30.54	1975.0 ± 0.6	2150.5 ± 1.9	0.37 ± 0.08

and connected with the Atlantic Ocean, thus, is selected as the ocean end-member (Table 1).

2.6. Statistical analysis

All measurements of the samples in the laboratory experiments were conducted in triplicate. In other word, all DIC and δ^{13}C-DIC data are reported as the average of 3-injections from each sample or each sample port. Statistical analysis of data was performed using a one-way ANOVA with a 95% confidence interval.

3. Results and discussion

3.1. Analytical precision and repeatability of the multi-port valve

For the same stock seawater measurements in the nine ports, we obtained a total of 81 raw data in three rounds with three consecutive injections per port. Based on all 81 raw data without any drift correction, the precisions of DIC concentrations and δ^{13}C-DIC values were 1.95 μmol kg^{-1} and 0.06‰ (Fig. 3). These precisions may be viewed as the upper boundary of the method uncertainties, which are slightly better than or similar to the overall analytical precisions of DIC measurements from the traditional NDIR method (0.1%; Huang et al., 2012) and δ^{13}C-DIC from the single-port version of this system (0.09‰; Su et al., 2019). These results indicate that the DIC concentrations and δ^{13}C-DIC values from all ports are not significantly different from each other, which is also verified by the statistics analysis (ANOVA test, DIC: $p = 0.99$, $n = 81$; δ^{13}C-DIC: $p = 0.35$, $n = 81$). However, if we first averaged the three consecutive injections on each port and then applied statistical analysis to each round (that is, $n = 9$ for each round), the deviations were much reduced. The standard

Fig. 3. Measured DIC concentrations (upper panel) and δ^{13}C-DIC values (lower panel) of the stock seawater using the multi-port valve. The solid lines in the two panels represent the averaged DIC concentration and δ^{13}C-DIC value from CRDS. Three rounds with three consecutive injections per port for nine ports were measured. The error bar is the standard deviations of the three consecutive injections at each port. This analytical procedure of three rounds lasted a total of about 20 h.

Table 2
The raw data of DIC and δ^{13}C-DIC in the multi-port valve test.

Port	δ^{13}C-DIC (‰)			DIC (μmol kg^{-1})		
	Round 1	Round 2	Round 3	Round 1	Round 2	Round 3
C	−3.93	−4.00	−3.98	2032.0	2033.0	2033.8
D	−3.97	−3.98	−3.97	2031.8	2033.3	2035.3
E	−3.94	−3.92	−3.98	2030.6	2034.4	2032.7
F	−3.91	−3.97	−3.97	2032.3	2032.7	2034.8
G	−3.94	−3.94	−3.97	2030.4	2031.6	2034.6
H	−3.88	−3.99	−4.02	2031.7	2031.7	2033.2
I	−3.95	−3.97	−3.98	2034.5	2032.7	2034.4
J	−3.91	−3.98	−3.96	2030.9	2034.7	2035.1
K	−4.00	−3.99	−3.95	2032.1	2034.6	2034.6
Average	−3.94	−3.97	−3.98	2031.8	2033.2	2034.3
STD	0.04	0.02	0.02	1.2	1.2	0.9
Average	−3.97			2033.1		
STD	0.02			1.5		

Note: Each datum reported here is an average of 3 consecutive injections with the standard deviations shown in Fig. 3.

deviations of DIC and δ^{13}C-DIC between multi-port valves were 0.9—1.2 μmol kg^{-1} and 0.02—0.04‰, respectively (Table 2 and Fig. 3). Since during our analysis of standards and samples, we made three injections and then used the average of the three injections as the raw data for each standard or sample, the statistical analysis based on the 3-injection averaged data may reflect the true instrument performance better than those based on the individual 81 raw data. We argue that the average of 3-injection based statistics at least point to the potential precision and possibly accuracy this method can achieve if a suitable standardization method can be accomplished in the future. Since the ultimate performance of the instrument is also limited by the calibration and standards, for now, we are content with reporting the precision as better than 1.95 μmol kg^{-1} for DIC and 0.06‰ for δ^{13}C-DIC. Therefore, we conclude that our instrument setup and technique have achieved the goal of better than ±0.05‰ for δ^{13}C-DIC precision recommended by Global Ocean Observing System (Cheng et al., 2019) and have the possibility to be a convenient tool to measure the δ^{13}C-DIC samples both onboard and in the laboratory. However, as noted here, a suitable and long-term consistent standardization method is still to be evaluated. Currently, all our δ^{13}C-DIC values are based on NaHCO$_3$ standards analyzed by the U.C. Davis Stable Isotope Facility.

This system is compact, both lab- and field-deployable, and analyzes DIC and δ^{13}C-DIC values without any sample pretreatment. In contrast, for offline IRMS δ^{13}C-DIC analysis, samples need to be acidified to liberate CO$_2$, which then goes through a vacuum line to be purified and concentrated into small vials before IRMS analysis (Humphreys et al., 2015). However, our method and system only need an operator to replace the samples once the previous batch analysis is completed. This automation avoids labor-intensive monitoring and operation, which allows for continuous measurements around the clock. Moreover, because instrument drift is low (DIC only drifted 0.059% and δ^{13}C-DIC drifted 0.047‰ within 3 weeks), the 3 standards are run only once a day or once every two days, after which all the time is dedicated to samples analysis in all nine sample channels. Note that, the standards and samples are run in a sequence each with three injections and a complete run average about 6 h. This results in a theoretical maximum throughput capacity of 37 samples with three injections (or 3 replicate measurements) each day (e.g., total 126 runs = (5 standards + 37 samples) × 3, and each run needs about 11 min). However, if we allow a larger analytical uncertainty or use a larger sample volume (or both), we can set the instrument to only two injections or just one injection, then, we can run more samples per day.

However, our system normally analyzed less samples during routine sample analysis due to instrument down time over night and due to the intention of evaluating the system performance via analyzing multiple standards during the method development and evaluation stage. For example, during our recent analysis of 1200 samples from the California Current System (samples were taken during June—July and analysis was conducted
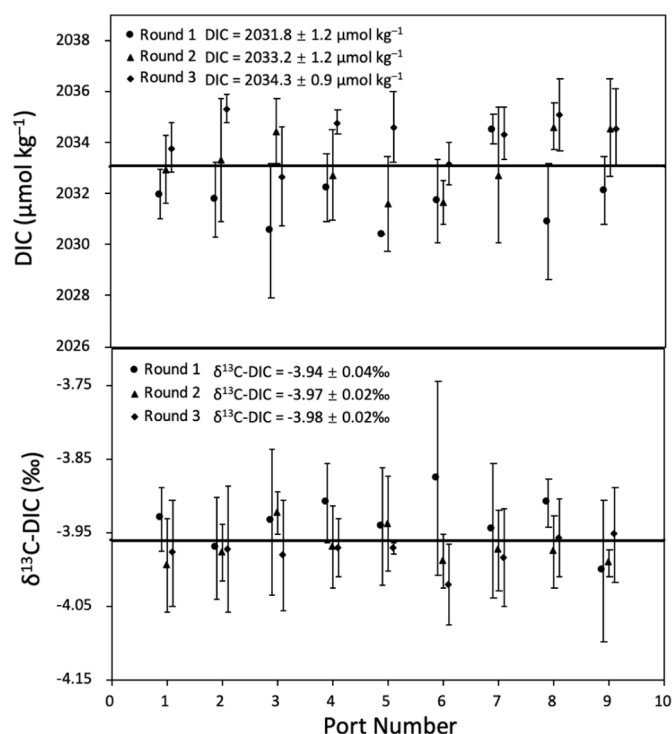
during August—early November 2021), 24 samples and two standards were analyzed each day with three shifts starting at ~8 am, ~3 pm and ~9 pm, respectively. During the overnight shift, the standards and some samples were analyzed twice. In addition to the home laboratory analysis, about 800 samples had been analyzed at sea onboard the research vessel Ron Brown during a 40-days cruise by two operators (on 12-h shifts). Compared with the analytical efficiency and application limitation of the IRMS instrument, our system greatly improves the spatial resolution of the δ^{13}C-DIC samples.

One potential issue that could affect the sample repeatability is the sample temperature. Although the Picarro G2131-i detector has a built-in temperature control mode to ensure the detector operates under stable thermal conditions to minimize the temperature effect on CO_2 and isotope detection, environmental temperature variations will still influence the density of the water sample and result in the uncertainty of carbon content in a fixed injection sample volume. In our study, all measurements were conducted in a temperature-controlled room ($T = 22 \pm 1$ °C), where the 1 °C temperature fluctuation will only cause a density change of 0.03% and an uncertainty of ± 0.5 μmol kg^{-1} in DIC concentration. It is smaller than the acceptable DIC precision of 2—4 μmol kg^{-1}, thus this temperature effect can be ignored. However, a water bath may be used onboard a ship or at a field laboratory to keep the sample temperature more stable.

3.2. Injection volume effect and concentration effect experiments

For the CRDS detector, the signals of CO_2 and $^{13}CO_2$ are determined by the carbon content liberated from water sample, rather than solely by the DIC concentration or injection volume. A smaller injection volume with a fixed DIC concentration or a lower DIC concentration with a fixed injection volume would result in a smaller integrated net area and a lower CO_2 peak and less distributed points of $^{13}CO_2$ above the cutoff value, thereby

potentially reducing the precision of δ^{13}C-DIC. For example, with a fixed DIC concentration, the uncertainty of δ^{13}C-DIC will increase as the injection volume decreases, which is known as injection volume effect. With a fixed injection volume, δ^{13}C-DIC uncertainty is less than ± 0.2‰ when DIC concentration is above 360 μmol kg^{-1}, whereas it rapidly increases to >0.5‰ when DIC concentration is <130 μmol kg^{-1} in the study by Bass et al. (2012), which is known as the concentration effect. The same is true in our analysis. As an extreme case in our analysis, if the entire CO_2 curve is less than the cutoff CO_2 value, there will be no valid δ^{13}C-DIC. If there is only a small fraction of the CO_2 curve near the peak above the cutoff line, then, one would expect a higher uncertainty in the derived δ^{13}C-DIC.

To examine the potential volume effect on the performance of the analyzer, we analyzed the same seawater with 24 different sample volumes (again, for each volume, there were three consecutive injections). The pooled averaged DIC concentration was 2355.8 ± 2.8 μmol kg^{-1} as determined by reference to CRM #185 (Fig. 4b), which is close to the value (2353.1 ± 0.4 μmol kg^{-1}) measured by the traditional NDIR method (Huang et al., 2012). Except for a few points near the low injection volume, all the DIC data fall within the precision range of $\pm 0.2\%$, which is only slightly higher than that of the traditional NDIR method (Huang et al., 2012). The averaged δ^{13}C-DIC was -5.56 ± 0.06‰ (Fig. 4a), again with high precision same as that in the multi-port evaluation. To be specific, 77.8% of the δ^{13}C-DIC data located in the averaged $\pm 1\sigma$ ranges if following our system precision (0.06%) while 91.7% of δ^{13}C-DIC data fall in the averaged $\pm 1\sigma$ ranges according to the precision (0.09%) of Su et al. (2019). We suggest that our measurement system is still stable even if the injection volume varies greatly. As mentioned above, the CO_2 and $^{13}CO_2$ signal are measured based on the carbon content of a sample. In the injection volume and concentration effect experiments, DIC and its δ^{13}C-DIC data are basically stable in a wide range of injection volume, which could be attributed to the fact that the stock seawater used in this experiment represents the
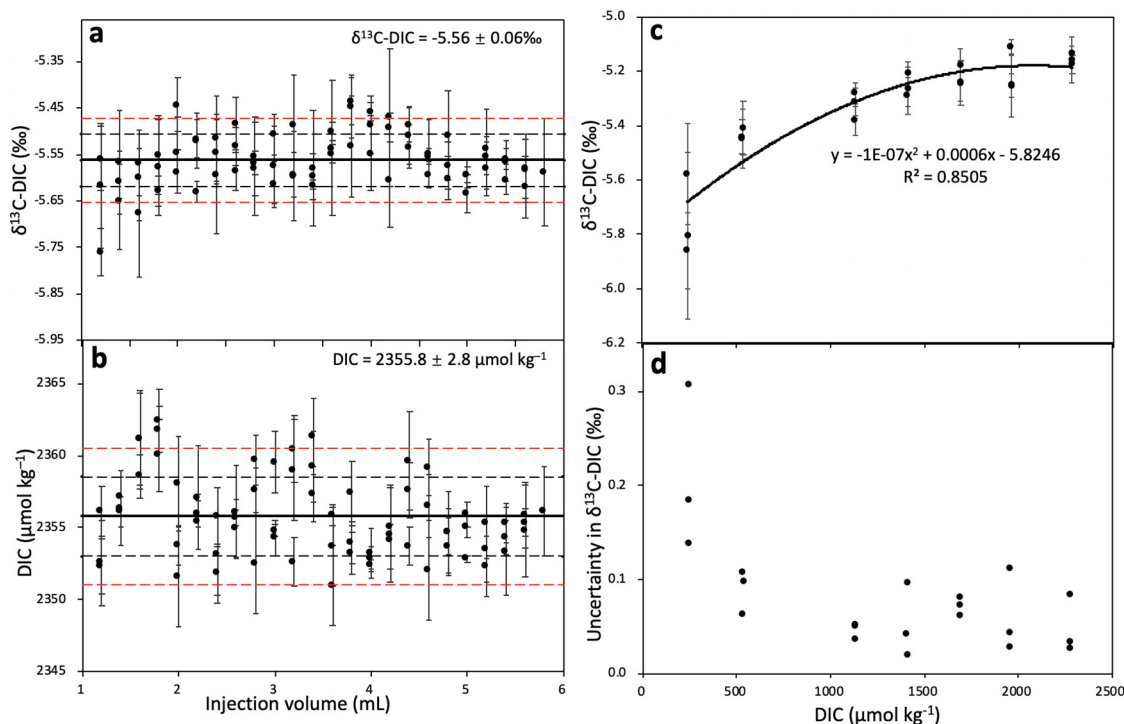

Fig. 4. δ^{13}C-DIC values and its precision (a) as well as measured DIC concentrations (b) of the aged seawater in the injection volume effect experiment; concentration effect on δ^{13}C-DIC values (c) and δ^{13}C-DIC uncertainty vs. DIC concentration (d) in the concentration effect experiment. In Fig (a) and (b), the black solid-lines indicate the averaged values of δ^{13}C-DIC values and DIC concentrations; For all data, the black dashed-lines represent 1 σ standard deviation interval; the red dashed-lines indicate 0.09‰ range for δ^{13}C-DIC and 2 σ standard deviation interval for DIC. In Fig (c), the black curve represents the relationship between the δ^{13}C-DIC values and DIC concentrations. Each injection volume and concentration have three repeat samples, and error bar means the standard deviations of the three injections for each sample. Note that these two experiments were two separate sets that ran on different days and were merged here together. Specifically, the injection volume effect experiment lasted about 64 h and the concentration effect experiment lasted about 35 h, the instrument always ran well during the intervals of these days (7 days).

typical open ocean water and has a high carbon content (DIC = 2355.8 μmol kg^{-1}). However, if estuarine water (such as DIC = ~1000 μmol kg^{-1} or less) is used for this experiment, the stability of δ^{13}C-DIC will be poor due to its low carbon content and few data points above the cutoff line. Therefore, the injection volume has a significant influence on the estuarine and riverine water with low DIC concentrations and a large injection volume will be needed to analyze δ^{13}C-DIC with high precision and accuracy.

For the concentration effect experiment, the δ^{13}C-DIC value exhibited a decreasing trend with a decreased DIC concentration, and the δ^{13}C-DIC became slightly depleted when DIC concentration decreased to 247 μmol kg^{-1} (Fig. 4c). The standard deviation of all δ^{13}C-DIC values was 0.20‰, which is not negligible given that the measurement precision of our measurement system is better than 0.06‰. However, except the lowest concentration of 247 μmol kg^{-1}, the isotope precision variation was small and better than 0.10‰ when DIC concentration ranged from 536 to 2283 μmol kg^{-1} (Fig. 4d), which is similar to the precision of Su et al. (2019) and also closer to our system precision. The lower δ^{13}C-DIC in lower DIC concentration could likely be attributed to the invasion of atmospheric CO_2 with lighter isotope during the pre-treatment process of the stock seawater dilution, which thus has a significant concentration effect on lower DIC concentration samples, compared with higher DIC concentration samples as Call et al. (2017) suggested before. Similarly, an obviously negative correlation between δ^{13}C-DIC values and DIC concentrations in the concentration effect for the δ^{13}C-DIC experiment in Prof. Wallace's lab at Dalhousie University also verified the invasion of atmospheric CO_2 in the preparation of a set of $NaHCO_3$ standard solution, since atmospheric CO_2 has a heavier isotope compared with −21.04‰ $NaHCO_3$ (Lin Cheng and D. Wallace, personal communications).

Here we offer an alternative explanation. As the carbon amount becomes lower either because of low sample volume or low DIC concentration, the weight of $\delta^{13}CO_2$ with higher instrument noise at lower $^{12}CO_2$ concentration (near 350 ppm) becomes more significant. We have noticed that such noise at low CO_2 level of a Picarro instrument is not necessarily random and may be instrument specific (for the two G2131-i units in our laboratory, one goes to more positive and another goes to more negative). Thus, we recommend maximizing the sample volume when DIC concentration of the sample is low.

While not fully and purposely evaluated, results from the volume and concentration experiments also indicate that there is no visible isotope fractionation effect in our instrument and method. Since we have selected a fixed criteria for ending sample analysis (when baseline after the peak is <5 ppm CO_2 above the baseline before the peak) and the cutoff CO_2 reading for averaging the $\delta^{13}CO_2$ value is fixed at 350 ppm (though both are user definable), the higher the DIC amount in the sample (either larger volume or higher concentration or both), the less $\delta^{13}CO_2$ signal is lost in counting toward the final δ^{13}C-DIC value. The fact that no statistically significant

difference is observed beyond ±0.06‰ when seawater sample volume is >2 mL (DIC is about 2000 μmol kg^{-1}) suggests that no significant isotope fractionation occurs in our method. It also appears that the same conclusion can be drawn for estuarine and freshwater analysis when the DIC concentration is above 500 μmol kg^{-1} (injection volume is 3.5 mL) and a slightly larger uncertainly of ±0.1‰ uncertainty is permitted. For analysis of freshwater samples with lower DIC, we recommend using a larger sample injection volume of 5.0 mL or greater.

3.3. Carbonate system in the Delaware Estuary

Compared with other large estuary systems like the Chesapeake Bay, the physical circulation and hydrology in the Delaware Estuary are relatively simple, because the major inflow is a single river and water is generally vertically well-mixed (Sharp et al., 1986). Thus, the Delaware Estuary is an ideal site for method development and evaluation, and has served this purpose well as a backyard laboratory for researchers at the University of Delaware for decades (Joesoef et al., 2015, 2017; Sharp, 1984; Sharp, 2010; Sharp et al., 1986, 2009).

The measured DIC and TA, pH_25°C and δ^{13}C-DIC increased while underway pCO$_2$ decreased with the increasing salinity from the upper tidal river to the low bay (Fig. 5). Specifically, from the river end to the ocean end, DIC increased from 970.6 to 1975.0 μmol kg^{-1}, TA increased from 944.6 to 2150.5 μmol kg^{-1}, and δ^{13}C-DIC increased from −9.57 to 0.37‰. DIC and TA had slightly higher values than the conservative mixing lines in the turbidity maximum zone. However, DIC concentrations were slightly lower than the conservative mixing line and TA values followed the conservative mixing line in the mid-salinity upper bay (Fig. 5a).

The δ^{13}C-DIC values along the salinity gradient were depleted in the freshwater areas, while enriched in the mid-salinity zone of the estuary (Fig. 5b). The pH_25°C and underway pCO$_2$ values were in the ranged from 7.61–8.10 and 1010–258 μatm, respectively, with marked salinity gradient changing from 0.16 to 30.54 (Fig. 5b and a). To be specific, pH increased from 7.61 in the Delaware River up to 8.10 in the upper bay, then decreased slightly to 7.95 in the marine part of the estuary. Compared to the atmospheric level (420 μatm), pCO$_2$ was obviously supersaturated (>500 μatm) in the turbidity maximum zone and then decreased to undersaturated in the mid and low bay. Consistent with pH distribution, pCO$_2$ value was lowest in the mid-salinity upper bay and slightly increased to near the atmospheric CO_2 level in the lower bay (Fig. 5a). Overall, the Delaware Estuary is characterized as a strong CO_2 source to the atmosphere in the river end and at the turbidity maximum zone and a weak CO_2 sink in the mid and lower bays during springtime. This observation is consistent with the investigation of Joesoef et al. (2015).

While it is clear that physical mixing plays the most important role in the Delaware Estuary, the deviations of carbonate parameters from the conservative mixing lines (Fig. 5) indicate that processes other than physical
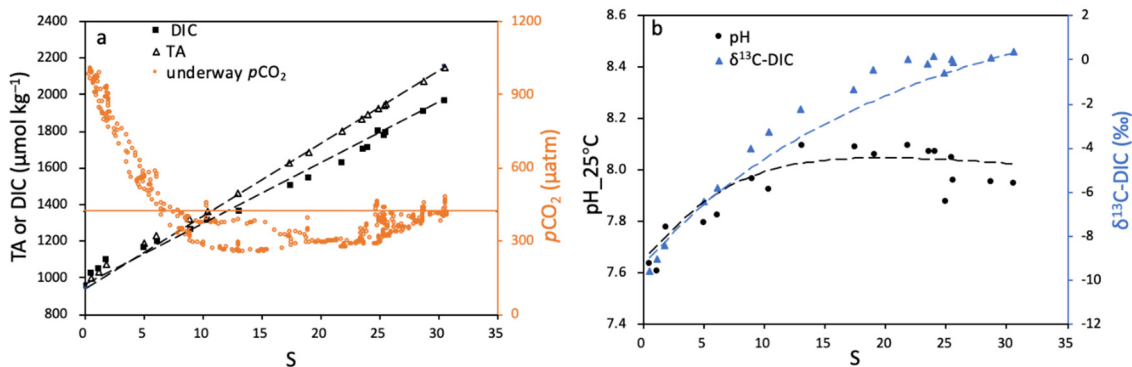

Fig. 5. Distributions of DIC and TA concentrations and underway pCO$_2$ (a), pH_25°C and δ^{13}C-DIC (b) against salinity. In Fig. 5a, the black dashed lines are the DIC and TA conservative mixing lines, the orange horizontal line represents the atmospheric pCO$_2$ level. In Fig. 5b, the black and blue dashed curves are the pH and δ^{13}C-DIC conservative mixing lines, respectively. The DIC, TA, pH_25°C and δ^{13}C-DIC conservative mixing lines are specified in Section 2.5.

mixing also play an important role in regulating their distributions in the estuary. While DIC distribution and dynamics have been studied by Joesoef et al. (2017), δ^{13}C-DIC has not been studied and could add an important constraint to identifying biogeochemical mechanisms important in controlling the carbon cycling and air-sea CO_2 flux. Therefore, in order to discuss the influencing mechanism of other processes on the DIC and its isotope distributions in the Delaware Estuary, the deviations of DIC concentrations and δ^{13}C-DIC signals from the above conservative mixing lines are used here for discussion, since the processes affecting DIC will have distinct δ^{13}C-DIC source values and isotope fractionation. Following the method described in Alling et al. (2012), the deviations of DIC concentrations and δ^{13}C-DIC signals from their conservative mixing lines (Eqs. (4) and (5)) can be calculated by the equations:

$$\Delta DIC = \frac{DIC_{meas} - DIC_{mix}}{DIC_{mix}} \tag{6}$$

$$\Delta\delta^{13}C-DIC = \delta^{13}C-DIC_{meas} - \delta^{13}C-DIC_{mix} \tag{7}$$

where DIC_{mix} and δ^{13}C-DIC$_{mix}$ are given in Eqs. (4) and (5), respectively. The main biogeochemical mechanisms affecting the distributions of δ^{13}C-

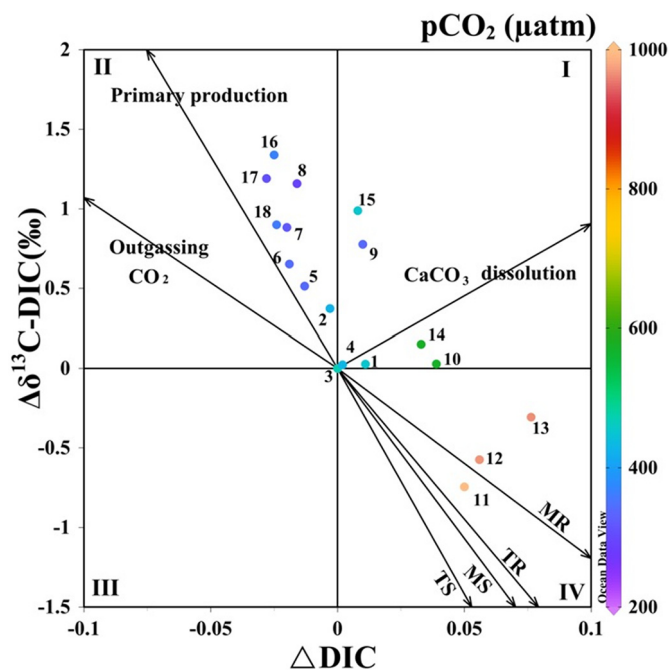**Fig. 6.** The absolute changes of δ^{13}C-DIC ($\Delta\delta^{13}$C-DIC) and the relative changes of DIC concentration (ΔDIC) relative to the conservative mixing lines in the Delaware Estuary in April 2019. The origin represents the data only controlled by physical mixing. The figure is divided into four quadrants, each indicating the position of samples whose DIC concentration and δ^{13}C-DIC were influenced by additional processes (non-physical mixing process). Quadrant I represents carbonate dissolution when both DIC and δ^{13}C-DIC increase; quadrant II represents primary production or CO_2 outgassing when DIC decreases while δ^{13}C-DIC increases; quadrant III represents $CaCO_3$ precipitation when both DIC and δ^{13}C-DIC decrease; quadrant IV represents degradation of organic carbon when DIC increases but δ^{13}C-DIC decreases. The vectors indicate the effects of most likely processes affecting DIC. Four vectors in quadrant IV indicate four possible effects of organic matter degradation, which depend on the sources of organic carbon (T: terrestrial source; M: marine source) and the initial DIC and δ^{13}C-DIC composition in the water (S: seawater; R: river water). MR (or TR) stands for CO_2 addition from the decomposition of marine (or terrestrial) organic matter to river water and MS (or TS) stands for CO_2 addition from the decomposition of marine (or terrestrial) organic matter to seawater. Arabic numerals in the figure represent the sampling stations. The calculations of all vectors are based on Samanta et al. (2015).

DIC and DIC could be inferred by the slopes of the relationship between $\Delta\delta^{13}$C-DIC and ΔDIC (Fig. 6).

Stations near the Delaware River fall within quadrant IV, which is characterized by the strong DIC addition and δ^{13}C-DIC depletion. It represents the influence of terrestrial organic matter degradation and is confirmed by the oversaturated pCO$_2$ relative to atmospheric CO_2 (Fig. 5a) and relatively low pH (Fig. 5b) (Cotovicz et al., 2019; Jiang et al., 2008; Yang et al., 2018). Meanwhile, low aragonite saturation state ($\Omega_{arag.}$ <0.37, Fig. 7) near the freshwater area indicates that $CaCO_3$ dissolution might also occur, which added to both DIC and TA, and in the meantime, enriched the δ^{13}C-DIC value by releasing the ^{13}C-enriched carbonate and bicarbonate ions into the water column DIC pool (Samanta et al., 2015). Therefore, the points in quadrant IV slightly deviate from the theoretical vector of terrestrial organic matter decomposition from the river source and shifted upward to the direction of the vector of $CaCO_3$ dissolution. Note that while the stoichiometric ratio of ΔTA to ΔDIC should be 2:1 during $CaCO_3$ dissolution, if the dissolution is driven by metabolically produced CO_2 input, then the ratio would be nearly or less than 1:1 (i.e., metabolic carbonate dissolution, $CaCO_3 + CH_2O + O_2 + H_2O \rightarrow Ca^{2+} + 2HCO_3^-$) (Burdige et al., 2008), which occurs near the freshwater endmember with S < 3 (Fig. 7).

The turbidity maximum zone stations are in the lower portion of quadrant I, mainly affected by $CaCO_3$ dissolution of suspended particulate matter and organic matter degradation. Additional evidence supporting the $CaCO_3$ dissolution mechanism is the substantial additions of DIC and TA in the low salinity region (Fig. 7). The excess TA (ΔTA = TA$_{meas}$ − TA$_{mixing}$) in and near the turbidity maximum zone (5 < S < 10) may mainly come from the $CaCO_3$ dissolution. Here the ΔTA to ΔDIC ratio ranges 1.3–1.7 and is much higher than those at or near the river endmember (S < 2) (Fig. 7). Therefore, the variations of DIC and δ^{13}C-DIC in the turbidity maximum zone were mainly controlled by the combined effects of organic carbon degradation from rivers and $CaCO_3$ dissolution.

Almost all stations in the Delaware Bay, including the upper bay and the lower bay, are in quadrant II. The Delaware Estuary has an inverted funnel shape, and the upper bay is below the neck of funnel, where the bay becomes wider, water flow slows down, clarity improves and biological production increases (Joesoef et al., 2015, 2017; Sharp, 2010). In addition, small scale spring blooms with high primary production usually occur in the Delaware Bay in March and April, especially in the upper bay (Powell et al., 2012). The high primary production, associated with DIC uptake, preferentially removes lighter ^{12}C and enriches the water with the heavier
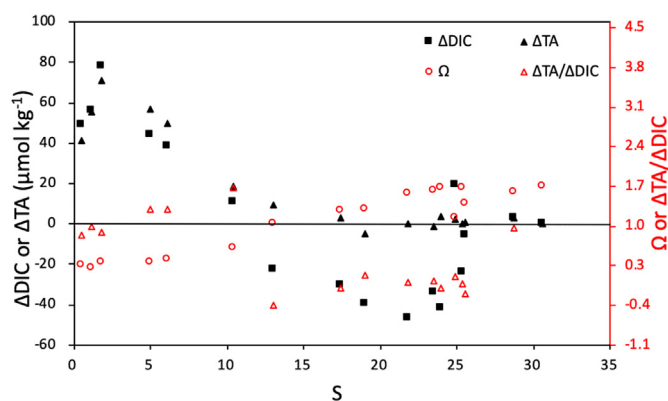

Fig. 7. The TA and DIC differences between measured and conservative mixing values (ΔTA and ΔDIC, left axis), aragonite saturation (Ω, right axis) and the ratio of ΔTA and ΔDIC (ΔTA/ΔDIC, right axis) against salinity. The black dashed horizontal line represents both the 0-reference line of ΔTA or ΔDIC, and the 1.0 aragonite saturation line. Data (solid square and triangle symbol) above the line mean addition, while beneath the line indicate removal of DIC or TA. Also, data (open circle symbol) above the line indicate conditions favoring calcium carbonate precipitation but dissolution below the line. Note we only present the saturation state of the more soluble mineral aragonite but another mineral calcite has a 1.5 times greater saturation state.

stable carbon isotope (Mook, 2001). Considering high biomass and primary productivity lead to undersaturated or nearly equilibrated pCO_2 relative to the atmospheric CO_2, there should be no impact from CO_2 outgassing. In addition, Stations 15 and 9 in the upper portion of the upper bay fall in the upper portion of quadrant I, which is dominated by the combined factors of primary production and $CaCO_3$ dissolution ($\Omega_{arag.}$ = 0.6 and 1.0, Fig. 7). Therefore, DIC loss and elevated δ^{13}C-DIC in the upper Delaware Bay are mainly attributed to primary production and $CaCO_3$ dissolution.

Although our calculations are associated with some uncertainties and limitations, the approach used in this study certainly provides a new insight into the sources and cycling of DIC in the Delaware Estuary and serves as a good example of using paired DIC concentrations and δ^{13}C-DIC values to study biogeochemical processes in aquatic systems. The deviations of DIC and δ^{13}C-DIC from conservative mixing lines can be regarded as fingerprints left by different biogeochemical processes. In particular, with the δ^{13}C-DIC data, we can now assess the role of $CaCO_3$ mineral dissolution, which we could not do during our past studies (Joesoef et al., 2017). Overall, the variations of the carbonate system are primarily controlled by the physical mixing in the Delaware Estuary. Besides that, the control mechanisms in the Delaware River and turbidity maximum zone are the combined effects of the degradation of organic carbon and carbonate dissolution, but are dominated by primary production in the Delaware Bay. The relative importance of these process changes over seasons, which will be the subject of a subsequent publication.

4. Conclusion

Here we extensively evaluated the performance of a method where we coupled a CO_2 extraction device with a multi-port sample valve and a CRDS detector to simultaneously analyze DIC concentrations and δ^{13}C-DIC values with high precision (better than ± 1.95 μmol kg^{-1} for DIC concentration and better than ± 0.06‰ for δ^{13}C-DIC). The highlight of the new instrument configuration is an upgraded multi-sample valve. The instrument setup can analyze 37 samples per day with three replicate measurements and achieve continuous measurements around the clock, which is convenient and labor-saving during analysis. Moreover, this instrument can be used in a variety of aquatic environments from rivers to open oceans to precisely analyze samples with different DIC concentrations.

This technique was applied in the Delaware Estuary in Spring of 2019 to determine the spatial distributions of DIC concentration and δ^{13}C-DIC. The relationship between ΔDIC and $\Delta\delta^{13}$C-DIC demonstrated that, in addition to estuarine mixing, carbonate chemistry was primarily controlled by the degradation of organic carbon and carbonate dissolution in the Delaware River and turbidity maximum zone, but mainly by primary production in the Delaware Bay. The application of this measuring system could rapidly expand the temporal and spatial coverages of the paired DIC concentration and δ^{13}C-DIC in the fieldwork, thereby facilitating further the understanding of the underlying biogeochemical processes and controls on air-sea CO_2 flux and acidification in different aquatic environments.

CRediT authorship contribution statement

Xue Deng: collect and process data, write and revise the manuscript.
Qian Li: collect data and review the manuscript.
Jianzhong Su: methodology, edit and review the manuscript.
Chun-Ying Liu: review the manuscript.
Eliot Atekwana: review the manuscript.
Wei-Jun Cai: Conceptualization, methodology, edit and review the manuscript, supervision.

Declaration of competing interest

The authors declare the following financial interests/personal relationships which may be considered as potential competing interests: W. -J. Cai is related to the Apollo SciTech.

References

Alling, V., Porcelli, D., Mörth, C.M., Anderson, L.G., Sanchez-Garcia, L., Gustafsson, Ö., Andersson, P.S., Humborg, C., 2012. Degradation of terrestrial organic carbon, primary production and out-gassing of CO_2 in the laptev and east siberian seas as inferred from δ^{13}C values of DIC. Geochim. Cosmochim. Acta 95, 143–159. https://doi.org/10.1016/j.gca.2012.07.028.

Atekwana, E.A., Krishnamurthy, R.V., 2004. Extraction of dissolved inorganic carbon (DIC) in natural waters for isotopic analyses. Handbook of Stable Isotope Analytical Techniques, pp. 203–228.

Bass, A.M., Bird, M.I., Munksgaard, N.C., Wurster, C.M., 2012. ISO-CADICA: Isotopic–continuous, automated dissolved inorganic carbon analyser. Rapid Commun. Mass Spectrom. 26, 639–644. https://doi.org/10.1002/rcm.6143.

Becker, M., Andersen, N., Fiedler, B., Fietzek, P., Körtzinger, A., 2012. Using cavity ringdown spectroscopy for continuous monitoring of δ^{13}C (CO_2) and fCO_2 in the surface ocean. Limnol. Oceanogr. Methods 10, 752–766. https://doi.org/10.4319/lom.2012.10.752.

Becker, M., Andersen, N., Erlenkeuser, H., Humphreys, M.P., Tanhua, T., Körtzinger, A., 2016. An internally consistent dataset of δ^{13}C-DIC in the North Atlantic Ocean–NAC13v1. Earth Syst. Sci. Data 8, 559–570. https://doi.org/10.5194/essd-8-559-2016.

Bhavya, P.S., Kumar, S., Gupta, G.V.M., Sudharma, K.V., Sudheesh, V., 2018. Spatio-temporal variation in δ^{13}CDIC of a tropical eutrophic estuary (Cochin estuary, India) and adjacent Arabian Sea. Cont. Shelf Res. 153, 75–85. https://doi.org/10.1016/j.csr.2017.12.006.

Burdige, D.J., Zimmerman, R.C., Hu, X., 2008. Rates of carbonate dissolution in permeable sediments estimated from pore-water profiles: the role of sea grasses. Limnol. Oceanogr. 53, 549–565. https://doi.org/10.4319/lo.2008.53.2.0549.

Call, M., Schulz, K.G., Carvalho, M.C., Santos, I.R., Maher, D.T., 2017. Technical note: coupling infrared gas analysis and cavity ring down spectroscopy for autonomous, high-temporal-resolution measurements of DIC and δ^{13}C–DIC. Biogeosciences 14, 1305–1313. https://doi.org/10.5194/bg-14-1305-2017.

Chen, B., Cai, W.-J., Brodeur, J.R., Hussain, N., Testa, J.M., Ni, W., Li, Q., 2020. Seasonal and spatial variability in surface pCO_2 and air–water CO_2 flux in the Chesapeake Bay. Limnol. Oceanogr. 65, 3046–3065. https://doi.org/10.1002/lno.11573.

Cheng, L., Normandeau, C., Bowden, R., Doucett, R., Gallagher, B., Gillikin, D.P., Kumamoto, Y., McKay, J.L., Middlestead, P., Ninnemann, U., Nothaft, D., Dubinina, E.O., Quay, P., Reverdin, G., Shirai, K., Mørkved, P.T., Theiling, B.P., van Geldern, R., Wallace, D.W.R., 2019. An international intercomparison of stable carbon isotope composition measurements of dissolved inorganic carbon in seawater. Limnol. Oceanogr. Methods 17, 200–209. https://doi.org/10.1002/lom3.10300.

Cotovicz, L.C., Knoppers, B.A., Deirmendjian, L., Abril, G., 2019. Sources and sinks of dissolved inorganic carbon in an urban tropical coastal bay revealed by δ^{13}C-DIC signals. Estuar. Coast. Shelf Sci. 220, 185–195. https://doi.org/10.1016/j.ecss.2019.02.048.

Dickinson, D., Bodé, S., Boeckx, P., 2017a. System for δ^{13}C–CO_2 and xCO_2 analysis of discrete gas samples by cavity ring-down spectroscopy. Atmos. Meas. Tech. 10, 4507–4519. https://doi.org/10.5194/amt-10-4507-2017.

Dickinson, D., Bodé, S., Boeckx, P., 2017b. Measuring ^{13}C-enriched CO_2 in air with a cavity ring-down spectroscopy gas analyser: evaluation and calibration. Rapid Commun. Mass Spectrom. 31, 1892–1902. https://doi.org/10.1002/rcm.7969.

Dickson, A.G., Sabine, C.L., Christian, J.R., 2007. Guide to Best Practices for Ocean CO_2 Measurements. 3. PICES Special Publication 191pp.

Friedrichs, G., Bock, J., Temps, F., Fietzek, P., Körtzinger, A., Wallace, D.W.R., 2010. Toward continuous monitoring of seawater ^{13}C$O_2/^{12}$C$O2$ isotope ratio and pCO_2: performance of cavity ringdown spectroscopy and gas matrix effects. Limnol. Oceanogr. Methods 8, 539–551. https://doi.org/10.4319/lom.2010.8.539.

Fry, B., 2002. Conservative mixing of stable isotopes across estuarine salinity gradients: a conceptual framework for monitoring watershed influences on downstream fisheries production. Estuaries 25, 264–271. https://doi.org/10.1007/BF02691313.

Gruber, N., Keeling, C.D., Stocker, T.F., 1998. Carbon-13 constraints on the seasonal inorganic carbon budget at the BATS site in the northwestern Sargasso Sea. Deep-Sea Res. I 45, 673–717. https://doi.org/10.1016/S0967-0637(97)00098-8.

Hellings, L., Dehairs, F., Tackx, M., Keppens, E., Baeyens, W., 1999. Origin and fate of organic carbon in the freshwater part of the scheldt estuary as traced by stable carbon isotope composition. Biogeochemistry 47, 167–186. https://doi.org/10.1007/BF00994921.

Huang, W.-J., Wang, Y., Cai, W.-J., 2012. Assessment of sample storage techniques for total alkalinity and dissolved inorganic carbon in seawater: sample storage techniques for TA and DIC. Limnol. Oceanogr. Methods 10, 711–717. https://doi.org/10.4319/lom.2012.10.711.

Humphreys, M.P., Achterberg, E.P., Griffiths, A.M., McDonald, A., Boyce, A.J., 2015. Measurements of the stable carbon isotope composition of dissolved inorganic carbon in the northeastern Atlantic and nordic seas during summer 2012. Earth Syst. Sci. Data 7, 127–135. https://doi.org/10.5194/essd-7-127-2015.

Jiang, L.-Q., Cai, W.-J., Wang, Y., 2008. A comparative study of carbon dioxide degassing in river- and marine-dominated estuaries. Limnol. Oceanogr. 53, 2603–2615. https://doi.org/10.4319/lo.2008.53.6.2603.

Joesoef, A., Huang, W.-J., Gao, Y., Cai, W.-J., 2015. Air–water fluxes and sources of carbon dioxide in the Delaware estuary: spatial and seasonal variability. Biogeosciences 12, 6085–6101. https://doi.org/10.5194/bg-12-6085-2015.

Joesoef, A., Kirchman, D.L., Sommerfield, C.K., Cai, W.-J., 2017. Seasonal variability of the inorganic carbon system in a large coastal plain estuary. Biogeosciences 14, 4949–4963. https://doi.org/10.5194/bg-14-4949-2017.

Kanamori, S., Ikegami, H., 1980. Computer-processed potentiometric titration for the determination of calcium and magnesium in sea water. J. Oceanogr. Soc. Jpn 36, 177–184. https://doi.org/10.1007/bf02070330.

Liu, S., Yang, S., Liu, M., Zhang, Y., Zhai, W., 2021. An optimization of the acid-extraction pretreatment procedure for precisely detecting stable isotopic composition of seawater dissolved inorganic carbon: its application in the bohai and yellow seas. Environ. Chem. 40, 2115–2124. https://doi.org/10.7524/j.issn.0254-6108.2020030104 (In Chinese with English abstract).

López-Sandoval, D.C., Delgado-Huertas, A., Carrillo-de-Albornoz, P., Duarte, C.M., Agustí, S., 2019. Use of cavity ring-down spectrometry to quantify ^{13}C-primary productivity in oligotrophic waters. Limnol. Oceanogr. Methods 17, 137–144. https://doi.org/10.1002/lom3.10305.

Mook, W.G., 2001. Environmental isotopes in the hydrological cycle. Principles and Applications. UNESCO, Paris.

Mucci, A., 1983. The solubility of calcite and aragonite in seawater at various salinities, temperatures, and one atmosphere total pressure. Am. J. Sci. 283, 780–799. https://doi.org/10.2475/ajs.283.7.780.

Pierrot, D., Lewis, E., Wallace, D.W.R., 2006. MS Excel Program Developed for CO_2 System Calculations. ORNL/CDIAC-105a. Carbon Dioxide Information Analysis Center, Oak Ridge National Laboratory, US Department of Energy, Oak Ridge, Tennessee 191pp.

Powell, E.N., Kreeger, D.A., Morson, J.M., Haidvogel, D.B., Wang, Z., Thomas, R., Gius, J.E., 2012. Oyster food supply in Delaware Bay: estimation from a hydrodynamic model and interaction with the oyster population. J. Mar. Res. 70, 469–503. https://doi.org/10.1357/002224012802851904.

Quay, P., Sonnerup, R., Westby, T., Stutsman, J., McNichol, A., 2003. Changes in the ^{13}C/^{12}C of dissolved inorganic carbon in the ocean as a tracer of anthropogenic CO_2 uptake. Glob. Biogeochem. Cycles 17, 1004. https://doi.org/10.1029/2001GB001817.

Quay, P.D., Stutsman, J., Feely, R.A., Juranek, L.W., 2009. Net community production rates across the subtropical and equatorial Pacific Ocean estimated from air-sea $δ^{13}$C disequilibrium. Glob. Biogeochem. Cycles 23, GB2006. https://doi.org/10.1029/2008GB003193.

Quay, P., Sonnerup, R., Munro, D., Sweeney, C., 2017. Anthropogenic CO_2 accumulation and uptake rates in the Pacific Ocean based on changes in the ^{13}C/^{12}C of dissolved inorganic carbon. Glob. Biogeochem. Cycles 31, 59–80. https://doi.org/10.1002/2016GB005460.

Salata, G.G., Roelke, L.A., Cifuentes, L.A., 2000. A rapid and precise method for measuring stable carbon isotope ratios of dissolved inorganic carbon. Mar. Chem. 69, 153–161. https://doi.org/10.1016/S0304-4203(99)00102-4.

Samanta, S., Dalai, T.K., Pattanaik, J.K., Rai, S.K., Mazumdar, A., 2015. Dissolved inorganic carbon (DIC) and its $δ^{13}$C in the ganga (Hooghly) river estuary, India: evidence of DIC generation via organic carbon degradation and carbonate dissolution. Geochim. Cosmochim. Acta 165, 226–248. https://doi.org/10.1016/j.gca.2015.05.040.

Schulte, P., van Geldern, R., Freitag, H., Karim, A., Négrel, P., Petelet-Giraud, E., Probst, A., Probst, J.-L., Telmer, K., Veizer, J., Barth, J.A.C., 2011. Applications of stable water and carbon isotopes in watershed research: weathering, carbon cycling, and water balances. Earth-Sci. Rev. 109, 20–31. https://doi.org/10.1016/j.earscirev.2011.07.003.

Sharp H, Jonathan, 1984. The Delaware Estuary: research as background for estuarine management and development. University of Delaware Sea Grant College Program.

Sharp, J.H., 2010. Estuarine oxygen dynamics: what can we learn about hypoxia from long-time records in the Delaware Estuary? Limnol. Oceanogr. 55, 535–548. https://doi.org/10.4319/lo.2010.55.2.0535.

Sharp, J.H., Cifuentes, L.A., Coffin, R.B., Pennock, J.R., Wong, K.-C., 1986. The influence of river variability on the circulation, chemistry, and microbiology of the Delaware estuary. Estuaries 9, 261–269. https://doi.org/10.2307/1352098.

Sharp, J.H., Yoshiyama, K., Parker, A.E., Schwartz, M.C., Curless, S.E., Beauregard, A.Y., Ossolinski, J.E., Davis, A.R., 2009. A biogeochemical view of estuarine eutrophication: seasonal and spatial trends and correlations in the Delaware estuary. Estuar. Coasts 32, 1023–1043. https://doi.org/10.1007/s12237-009-9210-8.

Su, J., Dai, M., He, B., Wang, L., Gan, J., Guo, X., Zhao, H., Yu, F., 2017. Tracing the origin of the oxygen-consuming organic matter in the hypoxic zone in a large eutrophic estuary: the lower reach of the Pearl River estuary, China. Biogeosciences 14, 4085–4099. https://doi.org/10.5194/bg-14-4085-2017.

Su, J., Cai, W.-J., Hussain, N., Brodeur, J., Chen, B., Huang, K., 2019. Simultaneous determination of dissolved inorganic carbon (DIC) concentration and stable isotope ($δ^{13}$C-DIC) by cavity ring-down spectroscopy: application to study carbonate dynamics in the Chesapeake Bay. Mar. Chem. 215, 103689. https://doi.org/10.1016/j.marchem.2019.103689.

Su, J., Cai, W.-J., Brodeur, J., Hussain, N., Chen, B., Testa, J.M., Scaboo, K.M., Jaisi, D.P., Li, Q., Dai, M., Cornwell, J., 2020. Source partitioning of oxygen-consuming organic matter in the hypoxic zone of the Chesapeake Bay. Limnol. Oceanogr. 65, 1801–1817. https://doi.org/10.1002/lno.11419.

Torres, M.E., Mix, A.C., Rugh, W.D., 2005. Precise δ13C analysis of dissolved inorganic carbon in natural waters using automated headspace sampling and continuous-flow mass spectrometry. Limnol. Oceanogr. Methods 3, 349–360. https://doi.org/10.4319/lom.2005.3.349.

Waldron, S., Scott, E.M., Vihermaa, L.E., Newton, J., 2014. Quantifying precision and accuracy of measurements of dissolved inorganic carbon stable isotopic composition using continuous-flow isotope-ratio mass spectrometry. Rapid Commun. Mass Spectrom. 28, 1117–1126. https://doi.org/10.1002/rcm.6873.

Wang, H., Dai, M., Liu, J., Kao, S.-J., Zhang, C., Cai, W.-J., Wang, G., Qian, W., Zhao, M., Sun, Z., 2016. Eutrophication-driven hypoxia in the East China Sea off the changjiang estuary. Environ. Sci. Technol. 50, 2255–2263. https://doi.org/10.1021/acs.est.5b06211.

Xuan, Y., Cao, Y., Tang, C., Li, M., 2020. Changes in dissolved inorganic carbon in river water due to urbanization revealed by hydrochemistry and carbon isotope in the Pearl River Delta, China. Environ. Sci. Pollut. Res. 27, 24542–24557. https://doi.org/10.1007/s11356-020-08454-4.

Yang, X., Xue, L., Li, Y., Han, P., Liu, X., Zhang, L., Cai, W.-J., 2018. Treated wastewater changes the export of dissolved inorganic carbon and its isotopic composition and leads to acidification in coastal oceans. Environ. Sci. Technol. 52, 5590–5599. https://doi.org/10.1021/acs.est.8b00273.